

Evolution of electrical conductivity and semiconductor to metal transition of iron oxides at extreme conditions

Yukai Zhuang(庄毓凯) and Qingyang Hu(胡清扬)

Citation: Chin. Phys. B, 2022, 31 (**8**): 089101. DOI: 10.1088/1674-1056/ac7557
Journal homepage: http://cpb.iphy.ac.cn; http://iopscience.iop.org/cpb

What follows is a list of articles you may be interested in

Elastic properties of $CaCO_3$ high pressure phases from first principles

Dan Huang(黄丹), Hong Liu(刘红), Ming-Qiang Hou(侯明强), Meng-Yu Xie(谢梦雨), Ya-Fei Lu(鹿亚飞), Lei Liu(刘雷), Li Yi(易丽), Yue-Ju Cui(崔月菊), Ying Li(李营), Li-Wei Deng(邓力维), Jian-Guo Du(杜建国)
Chin. Phys. B, 2017, 26 (**8**): 089101. DOI: 10.1088/1674-1056/26/8/089101

In-situ high pressure X-ray diffraction studies of orthoferrite $SmFeO_3$

Li Na-Na, Li Yan, Li Hui, Tang Rui-Lian, Zhao Yong-Sheng, Han Dan-Dan, Ma Yan-Mei, Cui Qi-Liang, Zhu Pin-Wen, Wang Xin
Chin. Phys. B, 2014, 23 (**6**): 069101. DOI: 10.1088/1674-1056/23/6/069101

In-situ high-pressure behaviors of double-perovskite Sr_2ZnTeO_6

Han Dan-Dan, Gao Wei, Li Na-Na, Tang Rui-Lian, Li Hui, Ma Yan-Mei, Cui Qi-Liang, Zhu Pin-Wen, Wang Xin
Chin. Phys. B, 2013, 22 (**5**): 059101. DOI: 10.1088/1674-1056/22/5/059101

TOPICAL REVIEW — Celebrating 30 Years of *Chinese Physics B*

Evolution of electrical conductivity and semiconductor to metal transition of iron oxides at extreme conditions

Yukai Zhuang(庄毓凯)[1] and Qingyang Hu(胡清扬)[2,†]

[1] *Institute of Atomic and Molecular Physics, Sichuan University, Chengdu* 610065, *China*
[2] *Center for High Pressure Science and Technology Advanced Research (HPSTAR), Beijing* 100094, *China*

(Received 6 April 2022; revised manuscript received 21 May 2022; accepted manuscript online 2 June 2022)

Iron oxides are widely found as ores in Earth's crust and are also important constituents of its interiors. Their polymorphism, composition changes, and electronic structures play essential roles in controlling the structure and geodynamic properties of the solid Earth. While all-natural occurring iron oxides are semiconductors or insulators at ambient pressure, they start to metalize under pressure. Here in this work, we review the electronic conductivity and metallization of iron oxides under high-pressure conditions found in Earth's lower mantle. We summarize that the metallization of iron oxides is generally controlled by the pressure-induced bandgap closure near the Fermi level. After metallization, they possess much higher electrical and thermal conductivity, which will facilitate the thermal convection, support a more stable and thicker D″ layer, and formulate Earth's magnetic field, all of which will constrain the large-scale dynamos of the mantle and core.

Keywords: high pressure, metallization, iron oxides, electrical conductivity

PACS: 91.60.Gf **DOI:** 10.1088/1674-1056/ac7557

1. Introduction

The chondritic planetary model calculates that the solid Earth consists of four major elements, which are 32.1 wt.% iron (Fe), 30.1 wt.% oxygen (O), 15.1 wt.% silicon (Si), and 13.9 wt.% magnesium (Mg).[1] The binary system of Fe–O covers more than half of Earth's weight. Thus, their high-pressure–temperature (*P*–*T*) properties play a vital role in understanding the dynamics and evolution of this planet. On Earth's surface, three natural occurring iron oxides are known since the Iron Age,[2] namely, FeO (wüstite, the ferrous state of iron), Fe_2O_3 (hematite, the ferric state of iron), and Fe_3O_4 (magnetite, mixed ferrous and ferric iron) which are used as ores for making iron. Tools obtained from iron smelting, a process that involves heating and chemical treatment to extract iron, have incubated symbolic civilizations in humans.[3]

While iron oxides at atmospheric pressure have been studied since more than 2600 years ago, the thermodynamical variable pressure brings forth even more intriguing physical and chemical phenomena. Under high pressure–temperature (*P*–*T*) conditions, several iron oxides with unconventional stoichiometries can exist through the chemistry of iron and naturally occurring iron oxides. For example, Fe_4O_5 is identified through x-ray diffraction at about 10 GPa and 1800 K,[4] and it possibly coexists with Fe_5O_6 at slightly higher temperatures (e.g., $\sim$2000 K).[5] Later on, complex iron-oxides with similar structural motifs like $Fe_{6.32}O_9$, Fe_7O_9, Fe_7O_{10}, and $Fe_{25}O_{32}$ are discovered at pressures throughout the lower mantle and they can also form solid solutions with Mg.[6–8] It is also worth noting that oxygen with a valence state greater than -2 can be stabilized under high pressure, as FeO_2 and $(Mg,Fe)O_2$ are identified at above 80 GPa.[9,10] Such wide chemistry flexibility makes iron-oxide one of the research frontiers in materials and Earth sciences.[11,12]

Our previous work has discussed the medium-range structural properties of the Fe–O system under high pressure.[13] Here in this work, we narrow down the scope to the electrical property of iron oxides, with a focus on its bandgap width under the influence of extreme conditions. While iron is a conventional metal, the other end-member of the Fe–O binary, oxygen also closes its bandgap at 96 GPa[14,15] and even becomes a superconductor at above megabar pressures.[16] For other members of iron oxides, previous laboratory electrical conductivity measurements show that they appear as semiconductors or insulators under ambient conditions. As the chemical bonding becomes stiffened under pressurization, their bandgap width generally becomes narrower in a response to electron hybridization and electrostatic interaction.[17] The critical metallization point is then constrained by the combination of thermodynamic parameters. During this process, the controlling conduction mechanism switches from small polaron (e.g., electron–hole hopping between Fe^{2+} and Fe^{3+}) to electron and ionic conduction.[18] It is also reported that the high-pressure polymorph of FeOOH enters the superionic state at above 80 GPa using the laser heating technique,[19] equivalent to the depth below $\sim$ 1800 km.[20–22] On account of the complex behavior of iron oxides, it is necessary to tease

†Corresponding author. E-mail: qingyang.hu@hpstar.ac.cn

© 2022 Chinese Physical Society and IOP Publishing Ltd

out the current research frontier of their evolution of electrical conductivity and semiconductor to metal transitions.

In this review, we first demonstrate the experimental and theoretical works in measuring the electrical conductivity of three natural-occurring iron oxides and their metallization conditions. We then summarize the latest progress in studying mix-valence mFeO·nFe$_2$O$_3$. We will also discuss the complex chemical and electronic properties of FeO_2. The last session discusses opportunities and challenges in this field of research. Each session will start with a simple introduction to the polymorphic transitions under high P–T conditions and followed by examples of electrical conductivity measurements. The evolution of high P–T electrical resistivity and the deep mantle metalized zones will be shown at the end of each session.

2. The archetypal wüstite FeO and challenges in describing strongly correlated iron oxides

Among the aforementioned iron oxides, wüstite (FeO) is an archetypal mineral to study strong correlation interaction and also a fundamental component in deep Earth. Under ambient conditions, FeO crystallizes in the NaCl-type (B1) structure. At pressure up to $\sim$ 16 GPa, B1 FeO exhibits lattice distortion along the [111] axis to the rhombohedral R structure (rB1).[23,24] In the deep lower mantle, the rB1 phase transforms to the NiAs-type (B8) phase at about 70 GPa after annealing at 1000 K.[25] Knittle *et al.* (1986) measured the resistance of B1 wüstite using the shock wave method. The resistivity has a negative correlation with pressure and reaches approximately the level of 10^{-6} Ω·m at 72 GPa and 1200 K, which may suggest the onset of metallization.[26] The metallic phase of FeO was then proved by x-ray diffraction and radiometric measurements.[27] Ohta *et al.* measured the electrical conductivity of both B1 and B8 FeO up to 169 GPa and 2050 K using a laser-heated diamond anvil cell. The temperature-dependent resistance measurements at 140 GPa and 150 GPa further demonstrate that B8 FeO is a metallic phase (Fig. 1).[28] The high-pressure Mössbauer studies on FeO (Fig. 2) show that the IS values of the nonmagnetic component decrease discontinuously in 114.5–131.1 GPa and the QS values also display a discontinuity in 109–131.1 GPa,[29] which is close to the metallization pressure range.

Other than experiments, theoretical studies have met major challenges in describing the electronic structure of FeO. Density functional theory (DFT) alone falsely predicts that FeO is metal under ambient conditions, and the problem is aided by correcting the exchange–correlation energies. For example, the first-order correction of Hubbard parameters works fairly well in reproducing the band structures.[30] However, the parameter U is the simplest approximation of exchange–correlation energies and the value may change by pressure and other thermodynamical variables. Varying pressure, U may reach different self-consistent values.[30] To remedy those issues, the dynamical mean-field theory (DMFT) is later combined with DFT to accurately predict the electronic structures of FeO. Most recent studies can reproduce its Mott insulator at ambient conditions with an energy gap of $\sim$ 2 eV and transformation to the metal state at about 60–70 GPa.[31–33]

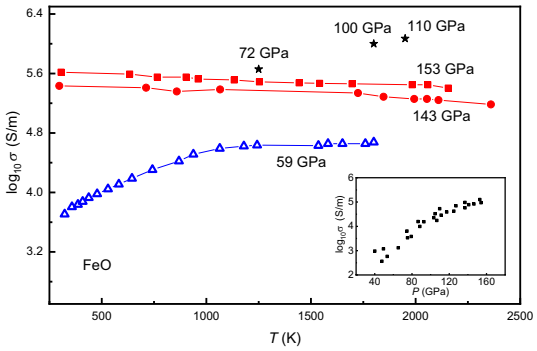


Fig. 1. The electrical conductivity of FeO at various temperatures. At 59 GPa, FeO is a semiconductor (blue symbol). The electrical conductivity of FeO decreases with the increasing temperature at above megabar pressures (red symbol), which is typical metallic behavior. The figure inset is the electrical conductivity variation of FeO as a function of pressure. Three black stars are from the shock wave experiment of Ref. [26], and the rest of the data are from the diamond anvil cell experiments of Ref. [28].

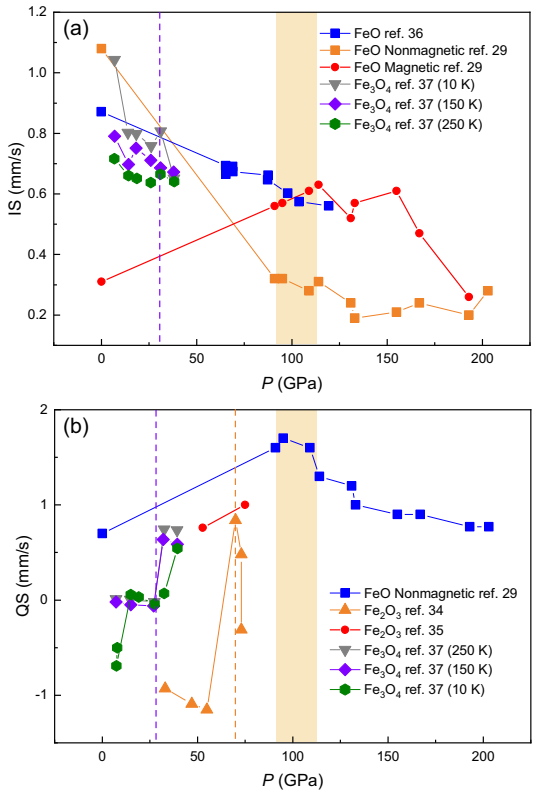


Fig. 2. The isomer shift (IS) and quadrupole splitting (QS) of iron oxides obtained from Mössbauer spectroscopy as functions of pressure.[29,34–37] The purple dotted line represents the possible phase transition of Fe_3O_4. The orange dotted line represents the possible phase transition of Fe_2O_3, and the orange area represents the phase transition region of FeO. The discontinuities of IS and QS values of iron oxides are used to indicates possible phase transitions.

3. Site-selective electronic transition in hematite Fe_2O_3

The structural phase diagram of ferrous hematite α-Fe_2O_3 (space group *Rc*) is more complicated than wüstite. It proceeds through a set of site-selective structural transformations under high *P*–*T* conditions.[7,34] The ambient α-Fe_2O_3 transforms to a Rh_2O_3-II-type (*Pbcn*) phase at 40 GPa and exhibits slight lattice distortion to a $GdFeO_3$-perovskite-type (*Pbnm*) phase at 50 GPa. High-pressure polymorphs of Fe_2O_3 contain the post-perovskite η-Fe_2O_3 (*Cmcm*) and a metastable orthorhombic θ-Fe_2O_3 (*Aba*2).[7,38–40] Both of them are stable in a wide pressure range of 60–120 GPa, which covers the entire deep lower mantle.

At ambient pressure, α-Fe_2O_3 is a wide-gap Mott insulator with a bandgap width of 2.0–2.7 eV, where the 0.7 eV bandgap range is inferred from different studies.[41,42] Recent DFT+DMFT results show that the closure of the bandgap under pressure is due to the iron and oxygen band broadening and the FeO_6 octahedra crystal-field splitting in e_g–t_{2g}. The bandgap closes at approximately 50 GPa in the Rh_2O_3-II-type phase, suggesting the onset of metallization.[43] Kune *et al.* predicted that the insulator–metal transition in Fe_2O_3 results from the gap closing mechanism[44] rather than the local state transition. The local state transition suggests that the insulator–metal transition is induced by the electron states transforming from localized to itinerant.[45]

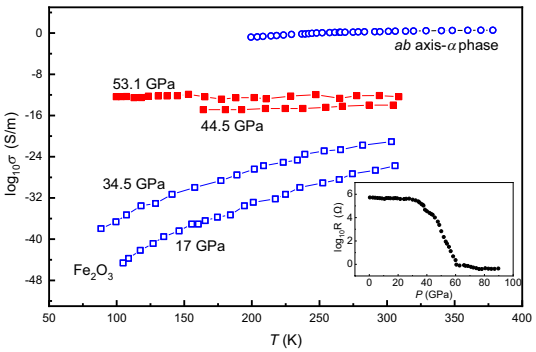


Fig. 3. Electrical conductivity of Fe_2O_3 with perovskite (square)[46] and α phase (circle).[48] Below decompression to 34.5 GPa, Fe_2O_3 is a semiconductor (black symbol). α-Fe_2O_3exhibits the same temperature behavior at ambient pressure. The temperature variation of electrical conductivity shows that perovskite type Fe_2O_3 becomes a metal at above 44.5 GPa (red symbol). The inset is the resistance of Fe_2O_3 as a function of pressure at 300 K,[46] which shows an abrupt decrease of about 6 orders of magnitude at 40–60 GPa.

Cold compressing a piece of Fe_2O_3 and measuring its electrical resistance measurements also show an abrupt 6 orders of magnitude decrease between 40 GPa and 60 GPa and the resistance reaches 1 Ω at above 60 GPa and ambient temperature (Fig. 3).[46] Greenberg *et al.* regarded the metallization as induced by a site-dependent collapse in the 3d electrons of iron (octahedral *B* sites).[46] For the *Aba*2 phase, Shim *et al.* employed Mössbauer spectroscopy and x-ray diffraction to show that Fe_2O_3 features reduced electron mobility near the Fermi level, which is evidence of strongly correlated metal (Fig. 2).[34] Such electronic structure transition is also implied by the x-ray absorption spectroscopy with the crystal-field splitting of the Fe *K* edge, indicating that Fe_2O_3 transforms from a high-spin insulator to a low-spin metal.[47]

4. Metallization of ferrous-ferric valence mixture magnetite Fe_3O_4

Magnetite (Fe_3O_4) is the oldest known magnetic material. It has an inverse spinel structure at ambient conditions, in which Fe^{3+} occupies the tetrahedral site and (Fe^{2+}, Fe^{3+}) holds the octahedral site. The ambient phase transforms to a high-pressure phase *Pbcm* at 29.7 GPa and 300 K,[49] and further to an orthorhombic phase (h-Fe_3O_4) with the $CaTi_2O_4$-type structure (*Bbmm*) at above 41 GPa and 1000 K or 65.1 GPa and 300 K,[50,51] where the Fe^{3+} is sixfold and the Fe^{2+} is eightfold coordinated in distorted FeO_6 octahedra.

Similar to FeO, a pioneering study using the full potential linear muffin-tin-orbital (FPLMTO) method also underestimates the bandgap of magnetite and h-Fe_3O_4.[50] Those theoretical results are against the pressure-dependent resistance measurements, in which Fe_3O_4 is a semiconductor until $\sim$ 50 GPa, where the resistance decreases rapidly and reaches a few Ω at above megabar pressure.[52] And at above $\sim$ 50 GPa, the resistance of h-Fe_3O_4 exhibits positive values of dR/dT with metallic features[50] (Fig. 4). At the same pressure, Mössbauer spectroscopy finds a correlation breakdown (Mott–Hubbard transition) of Fe^{3+} at $\sim$ 50 GPa, which suggests closure of the Fe-d and O-p gap.[52] Other Mössbauer study on Fe_3O_4 indicates a structural phase transition at about 30 GPa (Fig. 2).[37]

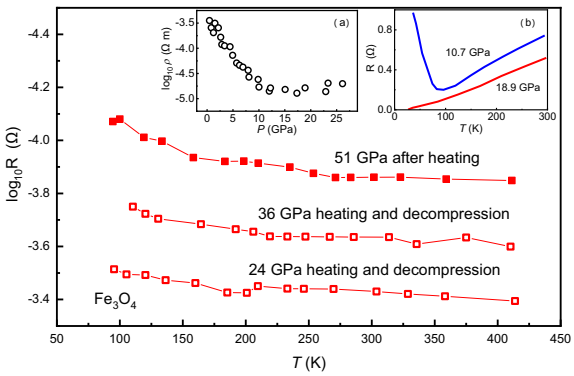


Fig. 4. The temperature-dependent resistance of high-pressure h-Fe_3O_4 after laser annealing. The solid red circles taken at 51 GPa are measured upon synthesis.[50] The open circles measured at lower pressures are pressure quenched from 51 GPa. It shows that the quenched metastable Fe_3O_4 keeps the metallic properties. The inset (a) is the resistance of Fe_3O_4 as a function of pressure at 300 K taken from Ref. [53], which is conducted up to 30 GPa. The data inset (b) is also the temperature-dependent resistance of Fe_3O_4 without heating, which show the metallic behavior at 18.9 GPa.[54]

So far, all three natural-occurring iron oxides are metalized under high pressure but their critical metallization pressure points are not correlated with their stoichiometry. Instead, the crystal structure becomes the controlling factor of their electronic structures. We sketch a semiconductor to metal phase diagram of the three iron oxides in Fig. 5. While we still lack experimental data points on the electrical conductivity of Fe_2O_3 before it decomposes to Fe_5O_7,[7] the diagram shows that the metalized areas of iron oxides are largely overlapped and cover large regions from the mid to the lowermost mantle.

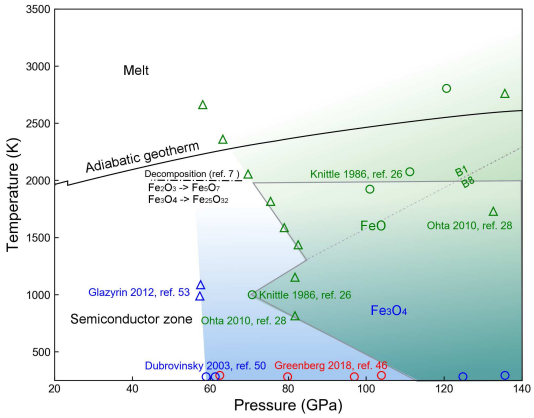


Fig. 5. Semiconductor to metal phase diagram of iron oxides. The translucent blue and green zones stand for the *P*–*T* regions of metallic FeO and Fe_3O_4, respectively. The data points are reported from literature.[7,26,28,46,50,53] Each color and symbol are labeled by the data points. The high-*P*–*T* electrical conductivity of Fe_2O_3 is still unknown below its decomposition conditions. We use the adiabatic geotherm from Katsura.[55] Grey lines sketch the overlapping *P*–*T* regions of Fe_3O_4 and FeO.

5. Pilot studies of other mFeO·$n$$Fe_2O_3$ mixtures

Most of the recently reported unconventional stoichiometry of high-pressure iron oxides can be described as the mixed-valence state of FeO and Fe_2O_3, in the chemical formula of mFeO·$n$$Fe_2O_3$. For instance, Fe_4O_5 is 2FeO·Fe_2O_3. This mixed-valence structure can be expressed as building blocks of octahedral FeO_6 into a post-perovskite type Fe_2O_3 or the structural assembly of FeO_6 octahedra and FeO_6 trigonal prisms (Fig. 6).[7,8,56] Previous research suggests that the stability of Fe_4O_5 in the upper mantle extends to oxygen fugacity higher than the diamond stability field[57] and it also can form solid solutions with Mg^{2+} and Cr^{3+} in the deep Earth.[58] While Fe_5O_6 can be stable in the upper mantle with the oxygen fugacity in equilibrium with the diamond formed.[58] Other research focused on Fe_4O_5 and Fe_5O_6 showed that the stability of Fe_5O_6 is above 10 GPa and 1600 K. And Fe_4O_5 only exists at relatively low temperatures.[59]

Due to the similarity of basic structural motifs, the electronic structures of mFeO·$n$$Fe_2O_3$ resemble that of natural iron oxides. For example, DFT+DMFT calculation results reveal that the total density of states of Fe_5O_6 at the Fermi level is dominated by the Fe-3d bands and possesses bulky quasi-particle peaks, which indicates that Fe_5O_6 is metallic at high pressure.[60] Employing the same calculation method, the electronic conduction in Fe_4O_5 is constrained by the Fe-3d bands, which are dominant by the total density of states at the Fermi level E_F.[61] They conclude that Fe_4O_5 stays metallic nature from ambient conditions through the core-mantle boundary (up to 140 GPa).[61] Although more electronic investigations on these mFeO·$n$$Fe_2O_3$ mixtures are called, they should be expected to undergo similar electronic structure transitions which have the same electronic mechanism.

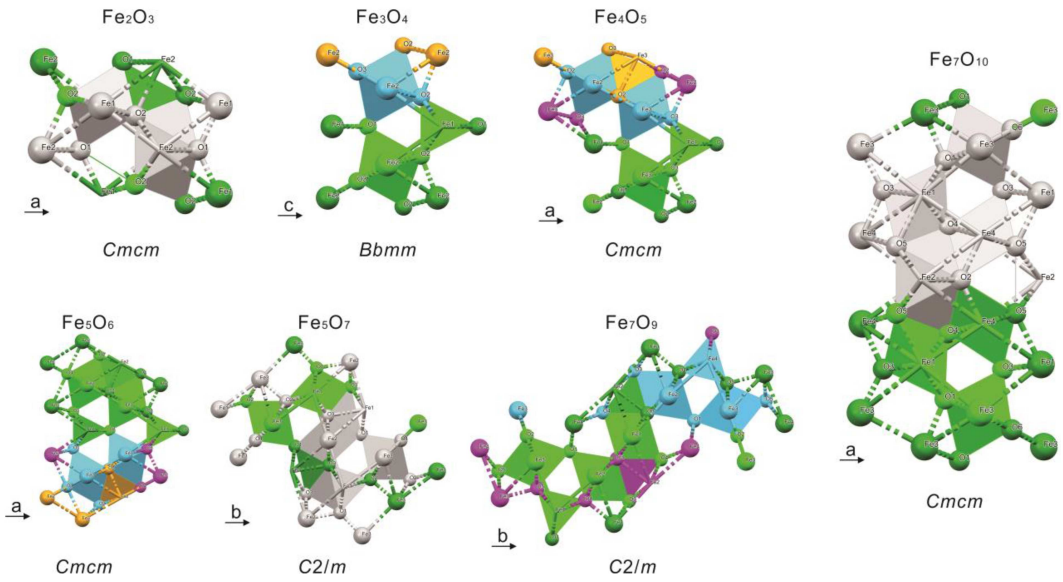


Fig. 6. The series of the high-pressure crystal structures of iron oxides with O^2. Brown colors represent octahedral FeO_6, while blue colors represent trigonal FeO_6. Different packing orders with face-shared and edge-shared FeO_6 blocks consist of high-pressure iron oxide phases with different crystal structures.

6. Complex bonding and electronic structure in oxygen-enriched FeO_2

Except for the iron oxides with usual O^2, FeO_2 with concurrent O^2 and O could be stable with a pyrite-type structure above 76 GPa and 1500 K, equivalent to approximately 1800 km depth.[9] Its crystal structure has co-existed Fe–O and O–O bonds and can be regarded as FeO holding extra O_2.[58] The synthesized FeO_2 has a semi-transparent color but it is still technically challenging to perform direct measurement on its bandgap.[9] In the meantime, DFT+DMFT calculations demonstrate that FeO_2 is a metal with wide overlapping of t_{2g} and σ^* bands.[62] From the derived density of states, the O_2 dimer adopts two electrons near an iron atom, causing its orbital to span approximately 3 eV right above the Fermi level. A following up work by the same theoretical group defines the electronic spin-state transition of Fe in FeO_2,[63] which explains the previous argument of Hubbard parameters U in modeling the system.[64] Coincidently, the metallization of FeO_2 is accompanied with spin transition,[63] which is also found in its hydrogen-bearing ε-FeOOH.[20]

7. Discussion and implication

Our review of previous works demonstrates that all iron oxides display metalized characteristics under high-pressure conditions. In Earth's deep interior, such metallization generally starts from the mid-lower mantle and keeps the metallic state at least to the lowermost mantle. Together with other components such as oxyhydroxide,[20,65] davemaoite ($CaSiO_3$),[66] and Al_2O_3[67] that are possible metals in the lower mantle, the deep Earth's interiors may feature high conductivity patches that generate electromagnetic phenomena and drive the geodynamics.

The electrical and thermal conductivities of the metalized minerals are coupled through the Wiedemann–Franz law.[68] Through this relation, the thermal conductivity is positively associated with the electrical conductivity of the metal. High thermal conductivity will facilitate the thermal convection, increase the heat flux, and finally influence the thermal dynamic at the mantle. The high thermal conductivity of metallic iron-oxides also implies a more stable and thicker D″ layer,[69] and an increase in plume temperature[70] that breaks through the phase boundary.

High electrical conductivity of metals will also heat certain areas at the base of the mantle, which will induce buoyancy to increase above the liquid outer core directly affecting the core dynamo process.[71,72] The strength of the magnetic field, which is largely determined by the core dynamo process, will be certainly influenced by the quasi-periodic variation. And the poloidal magnetic field structure at the lowest mantle will also be modified, or even determined by the high electrical conductivity. The energy of the poloidal magnetic field will increase with the rising conductivity of the mantle.[73]

8. Conclusions

In this work, we review the evolution of crystal and electronic structures of typical iron oxides and iron oxyhydroxides under high pressure conditions. Both theoretical and experimental works show that metallization is a universal phenomenon among those materials, whose bandgaps between the conduction band and valence band are closed by pressure. Meanwhile, their electrical conductivities soar to exhibit metallic behaviors. The metallic iron oxides represent an important class of materials for studying the electronic structures of strong-correlated matters. Its potential to form high electrical and thermal conductivity patches in the mantle will also impose profound influences on the dynamos of the mantle and core.

Acknowledgements

This work is supported by the National Natural Science Foundation of China (Grant Nos. 42150101 and 42150102). Qingyang Hu is supported by the CAEP Research Project (Grant No. CX20210048) and a Tencent Xplorer Prize (Grant No. XPLORER-2020-1013).

References

[1] Morgan J W and Anders E 1980 *Proc. Natl. Acad. Sci. USA* **77** 6973
[2] Schwertmann U and Taylor R M 1989 *Minerals in soil environments* (2nd edn.) (Madison: Soil Science Society of America) pp. 379–438
[3] Wagner D B 1995 *Philos. East West* **45** 136
[4] Lavina B, Dera P, Kim E, Meng Y, Downs R T, Weck P F, Sutton S R and Zhao Y 2011 *Proc. Natl. Acad. Sci. USA* **108** 17281
[5] Lavina B and Meng Y 2015 *Sci. Adv.* **1** e1400260
[6] Koemets E, Fedotenko T, Khandarkhaeva S, Bykov M, Bykova E, Thielmann M, Chariton S, Aprilis G, Koemets I, Glazyrin K, Liermann H P, Hanfland M, Ohtani E, Dubrovinskaia N, McCammon C and Dubrovinsky L 2021 *Eur. J. Inorg. Chem.* **2021** 3048
[7] Bykova E, Dubrovinsky L, Dubrovinskaia N, Bykov M, McCammon C, Ovsyannikov S V, Liermann H P, Kupenko I, Chumakov A I, Ruffer R, Hanfland M and Prakapenka V 2016 *Nat. Commun.* **7** 10661
[8] Sinmyo R, Bykova E, Ovsyannikov S V, McCammon C, Kupenko I, Ismailova L and Dubrovinsky L 2016 *Sci. Rep.* **6** 32852
[9] Hu Q, Kim D Y, Yang W, Yang L, Meng Y, Zhang L and Mao H K 2016 *Nature* **534** 241
[10] Hu Q, Liu J, Chen J, Yan B, Meng Y, Prakapenka V B, Mao W L and Mao H K 2021 *Natl. Sci. Rev.* **8** nwaa098
[11] Hu Q and Liu J 2021 *Geosci. Front.* **12** 975
[12] Mao H K and Mao W L 2020 *Matter Radiat. Extremes* **5** 038102
[13] Huang S and Hu Q 2022 *J. Appl. Phys.* **131** 070902
[14] Akahama Y, Kawamura H, Hausermann D, Hanfland M and Shimomura O 1995 *Phys. Rev. Lett.* **74** 4690
[15] Ma Y, Oganov A R and Glass C W 2007 *Phys. Rev. B* **76** 064101
[16] Shimizu K, Suhara K, Ikumo M, Eremets M I and Amaya K 1998 *Nature* **393** 767
[17] Yoo C S 2020 *Matter Radiat. Extrem.* **5** 018202
[18] Yoshino T 2009 *Surv. Geophys.* **31** 163

[19] Zhuang Y, Li J, Lu W, Yang X, Du Z and Hu Q 2022 *Chin. Phys. Lett.* **39** 020701
[20] Zhuang Y, Gan B, Cui Z, Tang R, Tao R, Hou M, Jiang G, Popescu C, Garbarino G, Zhang Y and Hu Q 2022 *Sci. Bull.* **67** 748
[21] Hu Q and Mao H K 2021 *Matter Radiat. Extrem.* **6** 068101
[22] Hou M, He Y, Jang B G, Sun S, Zhuang Y, Deng L, Tang R, Chen J, Ke F, Meng Y, Prakapenka V B, Chen B, Shim J H, Liu J, Kim D Y, Hu Q, Pickard C J, Needs R J and Mao H k 2021 *Nat. Geosci.* **14** 174
[23] Ono S, Ohishi Y and Kikegawa T 2007 *J. Phys.-Condens. Mat.* **19** 036205
[24] Ding Y, Cai Z, Hu Q, Sheng H, Chang J, Hemley R J and Mao W L 2012 *Appl. Phys. Lett.* **100** 041903
[25] Ozawa H, Hirose K, Tateno S, Sata N and Ohishi Y 2010 *Phys. Earth Planet. In.* **179** 157
[26] Knittle E, Jeanloz R, Mitchell A C and Nellis W J 1986 *Solid State Commun.* **59** 513
[27] Fischer R A, Campbell A J, Lord O T, Shofner G A, Dera P and Prakapenka V B 2011 *Geophys. Res. Lett.* **38** L24301
[28] Ohta K, Hirose K, Shimizu K and Ohishi Y 2010 *Phys. Rev. B* **82** 174120
[29] Hamada M, Kamada S, Ohtani E, Mitsui T, Masuda R, Sakamaki T, Suzuki N, Maeda F and Akasaka M 2016 *Phys. Rev. B* **93** 155165
[30] Cococcioni M and de Gironcoli S 2005 *Phys. Rev. B* **71** 035105
[31] Shorikov A O, Pchelkina Z V, Anisimov V I, Skornyakov S L and Korotin M A 2010 *Phys. Rev. B* **82** 195101
[32] Leonov I 2015 *Phys. Rev. B* **92** 085142
[33] Zhang P, Cohen R E and Haule K 2017 *J. Phys. Conf. Ser.* **827** 012006
[34] Shim S H, Bengtson A, Morgan D, Sturhahn W, Catalli K, Zhao J, Lerche M and Prakapenka V 2009 *Proc. Natl. Acad. Sci. USA* **106** 5508
[35] Kupenko I, Aprilis G, Vasiukov D M, McCammon C, Chariton S, Cerantola V, Kantor I, Chumakov A I, Ruffer R, Dubrovinsky L and Sanchez-Valle C 2019 *Nature* **570** 102
[36] Pasternak M P, Taylor R D, Jeanloz R, Li X, Nguyen J H and McCammon C A 1997 *Phys. Rev. Lett.* **79** 5046
[37] Kozlenko D P, Dubrovinsky L S, Kichanov S E, Lukin E V, Cerantola V, Chumakov A I and Savenko B N 2019 *Sci. Rep.* **9** 4464
[38] Pasternak M P, Rozenberg G K, Machavariani G Y, Naaman O, Taylor R D and Jeanloz R 1999 *Phys. Rev. Lett.* **82** 4663
[39] Bykova E, Bykov M, Prakapenka V, Konôpková Z, Liermann H P, Dubrovinskaia N and Dubrovinsky L 2013 *High Press. Res.* **33** 534
[40] Rozenberg G K, Dubrovinsky L S, Pasternak M P, Naaman O, Le Bihan T and Ahuja R 2002 *Phys. Rev. B* **65** 064112
[41] Kim K H, Lee S H and Choi J S 1985 *J. Phys. Chem. Solids* **46** 331
[42] Mochizuki S 1977 *Phys. Stat. Sol. (a)* **41** 591
[43] Kunes J, Korotin D M, Korotin M A, Anisimov V I and Werner P 2009 *Phys. Rev. Lett.* **102** 146402
[44] Kunes J, Lukoyanov A V, Anisimov V I, Scalettar R T and Pickett W E 2008 *Nat. Mater.* **7** 198
[45] McMahan A K, Held K and Scalettar R T 2003 *Phys. Rev. B* **67** 075108
[46] Greenberg E, Leonov I, Layek S, Konopkova Z, PasternakMP, Dubrovinsky L, Jeanloz R, Abrikosov I A and Rozenberg G K 2018 *Phys. Rev. X* **8** 031059
[47] Wang S, MaoWL, Sorini A P, Chen C C, Devereaux T P, Ding Y, Xiao Y, Chow P, Hiraoka N, Ishii H, Cai Y Q and Kao C C 2010 *Phys. Rev. B* **82** 144428
[48] Ovsyannikov S V, Morozova N V, Karkin A E and Shchennikov V V 2012 *Phys. Rev. B* **86** 205131
[49] Ju S, Cai T Y, Lu H S and Gong C D 2012 *J. Am. Chem. Soc.* **134** 13780
[50] Dubrovinsky L S, Dubrovinskaia N A, McCammon C, Rozenberg G K, Ahuja R, Osorio-Guillen J M, Dmitriev V, Weber H P, Le Bihan T and Johansson B 2003 *J. Phys.-Condens. Mat.* **15** 7697
[51] Fei Y, Frost D J, Mao H K, Prewitt C T and Häusermann D 1999 *Am. Mineral.* **84** 203
[52] Xu W M, Machavariani G Y, Rozenberg G K and Pasternak M P 2004 *Phys. Rev. B* **70** 174106
[53] Glazyrin K, McCammon C, Dubrovinsky L, Merlini M, Schollenbruch K, Woodland A and Hanfland M 2012 *Am. Mineral.* **97** 128
[54] Muramatsu T, Gasparov L V, Berger H, Hemley R J and Struzhkin V V 2016 *J. Appl. Phys.* **119** 135903
[55] Katsura T 2022 *J. Geophys. Res.-Sol. Ea.* **127** e2021JB023562
[56] Guignard J and Crichton W A 2018 *Mineral. Mag.* **78** 361
[57] Hu Q and Mao H k 2021 *Matter Radiat. at Extremes* **6** 068403
[58] Myhill R, Ojwang D O, Ziberna L, Frost D J, Ballaran T B and Miyajima N 2016 *Contrib. Mineral. Petr.* **171** 51
[59] Hikosaka K, Sinmyo R, Hirose K, Ishii T and Ohishi Y 2019 *Am. Mineral.* **104** 1356
[60] Qin Q Y, Yang A Q, Tao X R, Yang L X, Gou H Y and Zhang P 2021 *Chin. Phys. Lett.* **38** 089101
[61] Yang A, Qin Q, Tao X, Zhang S, Zhao Y and Zhang P 2021 *Phys. Lett. A* **414** 127607
[62] Jang B G, Kim D Y and Shim J H 2017 *Phys. Rev. B* **95** 075144
[63] Jang B G, Liu J, Hu Q, Haule K, Mao H k, Mao W L, Kim D Y and Shim J H 2019 *Phys. Rev. B* **100** 014418
[64] Nishi M, Kuwayama Y, Tsuchiya J and Tsuchiya T 2017 *Nature* **547** 205
[65] Tang R, Liu J, Kim D Y, Mao H k, Hu Q, Yang B, Li Y, Pickard C J, Needs R J, He Y, Liu H, Prakapenka V B, Meng Y and Yan J 2021 *Sci. Bull.* **66** 1954
[66] Tsuchiya T and Tsuchiya J 2011 *Proc. Natl. Acad. Sci. USA* **108** 1252
[67] Nellis W J 2010 *Phys. Rev. B* **82** 092101
[68] Zhuang Y, Su X, Salke N P, Cui Z, Hu Q, Zhang D and Liu J 2021 *Geosci. Front.* **12** 983
[69] Goncharov A F, Haugen B D, Struzhkin V V, Beck P and Jacobsen S D 2008 *Nature* **456** 231
[70] Montague N L, Kellogg L H and Manga M 1998 *Geophys. Res. Lett.* **25** 2345
[71] van den Berg A P, Yuen D A, Beebe G L and Christiansen M D 2010 *Phys. Earth Planet. In.* **178** 136
[72] Chan K H, Zhang K, Li L and Liao X 2008 *Phys. Earth Planet. In.* **169** 204
[73] Vilim R, Stanley S and Elkins-Tanton L 2013 *Astrophys. J.* **768** L30